

Identification and Adjustment of Guide Rail Geometric Errors Based on BP Neural Network

Gaiyun He, Can Huang, Longzhen Guo, Guangming Sun, Dawei Zhang

Key Laboratory of Mechanism Theory and Equipment Design of Ministry of Education, Tianjin University, Tianjin 300072, China, hegaiyun@tju.edu.cn

The relative positions between the four slide blocks vary with the movement of the table due to the geometric errors of the guide rail. Consequently, the additional load on the slide blocks is increased. A new method of error measurement and identification by using a self-designed stress test plate was presented. BP neural network model was used to establish the mapping between the stress of key measurement points on the test plate and the displacements of slide blocks. By measuring the stress, the relative displacements of slide blocks were obtained, from which the geometric errors of the guide rails were converted. Firstly, the finite element model was built to find the key measurement points of the test plate. Then the BP neural network was trained by using the samples extracted from the finite element model. The stress at the key measurement points were taken as the input and the relative displacements of the slide blocks were taken as the output. Finally, the geometric errors of the two guide rails were obtained according to the measured stress. The results show that the maximum difference between the measured geometric errors and the output of BP neural network was 5 μm . Therefore, the correctness and feasibility of the method were verified.

Keywords: Guide rail geometric error, stress, the test plate, finite element model, BP neural network.

1. INTRODUCTION

The precision maintenance is one of the most important criteria of machine tools, which is affected by the stiffness, geometric errors and thermal errors [1]-[2]. After the machine tools assembly had been completed, the stress is gradually released with time. Thus, the precision of the machine tools cannot maintain a high level for a long time. The distribution of stress in machine tools is influenced by many factors, and the geometric error is one of the key factors.

The geometric errors of the guide rails mainly include the straightness and the parallelism between the two guide rails. In the manufacturing and installation process, linear rolling guide rail will inevitably produce errors, resulting in the relative position of four slider blocks changing with the table movement [3]. The stress generated within the guide system is thereby affecting the precision maintenance of the table.

Over the past decades, the geometric errors of guide rails and their influence on motion accuracy of the table have been studied. Mahdi Rahmani investigated the geometric accuracy and its effect on the performance of the guiding system in machine tools with finite element method [4]. Eiji Shamoto et al. used the transfer function model to establish the relationship between geometric errors of hydrostatic guide and table motion errors [5]. The geometric errors of

the guide rail were calculated by measuring motion errors of the table. Gyungho Khim et al. took linear rolling guide as the subject and established the force balance equation of the table using the same method. The calculations were carried out via the Hertz contact theory. In addition, the influence of the guide rail geometric errors on the 5-DOF motion errors was analyzed [6]-[7]. Gyu Ha Kim proposed a new transfer function method based on reaction force-moment model with a double spring system. The influence of the pitch error of the slide block on the moment was also considered [8]. However, the deformation of the table and the slide block was not considered in their research. It was deemed that omitting the elasticity of the table and slide block was an excessive simplification.

At present, the relationship between the deformation field and the distribution of stress is rarely researched. Li et al. presented a test method of assembly stress based on the strain test [9]. The stress distribution of the machine tools was studied in a different assembly process. The results showed that the tightening sequence of bolts has little influence on the assembly stress. Paolo Bosetti presented a novel measurement system for measuring deformation field of machine tools components [10]. The struts in the system were instrumented with a strain sensor which provided their longitudinal strain values. An algorithm was used to evaluate the discrete displacements filed by calculating the

node positions on the basis of the strut longitudinal deformations. Liu et al. employed optical fiber Bragg grating sensors to measure the strain field of machine tool components in real time [11]. The deformation field was obtained according to the structural dimension of the component. Consequently, the displacement of the tool tip was obtained.

The finite element method has been widely used in the engineering field. Edward Chlebus described a method of calculating the static performance of guide rails using the finite element analysis [12]. The effectiveness of the method of modeling and calculation was confirmed by experiments. Pawel Majda used the finite element method to study the relationship between kinematic straightness errors and angular errors of the table [13]. The simulation results showed that no close relationship was found between these two types of errors. Meanwhile, a method of analytical and experimental examinations to research the influence of the guide rail geometric errors on joint kinematic errors was proposed [14]. The results verified that the deformation of table could be a significant source of errors in volumetric error models. However, the relationship between the geometric errors of the guide rails and the stress distribution of the table has not been researched.

In this paper, a new measuring instrument and method were adopted to identify geometric errors of guide rails. The self-designed test plate was regarded as the elastic element. The stress state of the test plate was analyzed when the relative position of the slide blocks changed. The mapping relationship between relative displacements of slide blocks and the stress of the test plate were established by BP neural network. The measured stress of the test plate was input into the BP neural network. Consequently, the geometric errors of the two guide rails in X and Y directions can be obtained, which can provide the basis for the adjustment of the guide rail geometric errors.

2. THE STRUCTURE OF THE TEST PLATE

Due to the geometric errors of the guide rails, the relative displacements of sliders are produced during the movement. When the stiffness of the table is sufficient enough, the deformation occurs mainly on the slide blocks [15]. The additional load on the slide blocks was increased, which affects the useful life of the slide blocks and the precision maintenance of the table. When the stiffness of the table is insufficient, the table will deform greatly. And the stress state of the table will change with the relative displacements of the slide blocks. Because of the complex structure of the actual table, it is difficult to measure the stress. Therefore, a simplified test plate was designed as the stress measuring instrument. And the relative displacements of the slide blocks were reflected by the stress state of the test plate.

A. Structure of the test plate

According to the distance between the two guide rails, the length of the test plate l_m was designed to be 560 mm, the width l_w was 560 mm and the thickness l_t was 45 mm.

In order to highlight the stress in different directions on the surface of the test plate, the ribs were arranged in the form of the structure shown in Fig.1. Eight ribs were equally distributed on the test plate. The width of the ribs l_{rw} was 15 mm, the height l_{rh} was 25 mm. The angle α between the ribs was 45° .

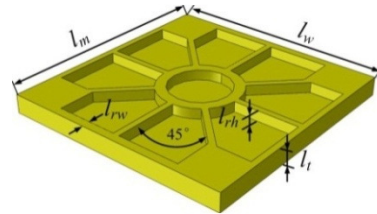


Fig.1. Basic dimensions of the test plate.

B. Stress comparison with different structures

In order to demonstrate the advantage of the test plate, we made a comparison with a flat plate. The flat plate has the same basic dimensions except that the thickness was 20 mm without ribs. The vertical displacement was applied to the contact surface between the test plate and the second slide block. The same vertical displacement was applied to the same position of the flat plate. In Fig.2., the stress nephogram of the two kinds of plates is compared. P_1, P_2, P_3, P_4 are the serial numbers of the slider blocks.

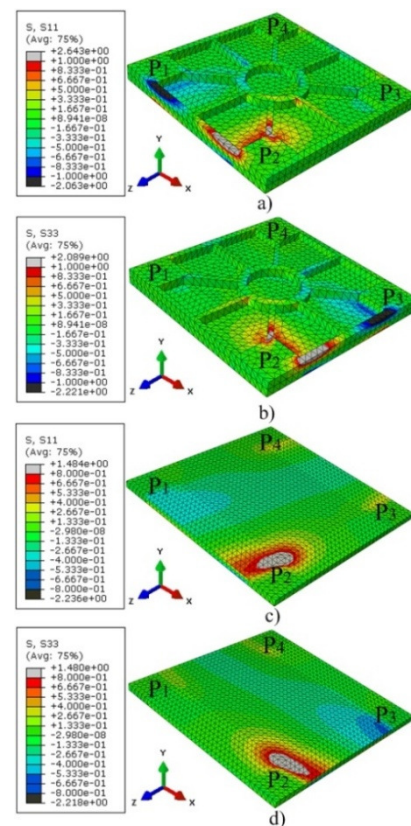


Fig.2. The stress nephogram of the plates when the vertical displacement was applied to the second contact surface. a) and b): the stress distribution of the test plate; c) and d): the stress distribution of the flat plate.

In Fig.2.a) and Fig.2.b), the stress is mainly distributed on the ribs and the direction of stress is consistent with the direction of the ribs. In Fig.2.c) and Fig.2.d), the stress in different directions is mainly distributed in a certain area. So, it is more convenient to measure the stress of the test plate. The stress state of the test plate will be changed with the relative displacements of the slide blocks, and then get the geometric errors of guide rails.

3. FINITE ELEMENT MODEL

In modeling, the finite element method (FEM) was used. The sub-assemblies were discretized with solid elements, which made it possible to allow the elasticity within the linear elastic range for guide rail, slide block, and test plate.

A. The roller contact stiffness

When the roller was subjected to a load, the elastic deformation occurred between the roller and the raceway. Considering the usefulness of the performed analytical examinations, it seemed that omitting the elasticity of single roller was an excessive simplification, which decreased the reliability of the performed analyses.

In the finite element model, the roller can be equivalent to the spring element [14]. Considering geometric non-linearity (only compression), the contact deformation of the single roller within two grooves can be calculated by the Palmgren empirical formula [16].

$$\delta = 1.36 \frac{(\eta Q_n)^{0.9}}{(l_e)^{0.8}} \quad (1)$$

$$\eta = \frac{1}{E'} = \frac{1-\nu_1^2}{E_1} + \frac{1-\nu_2^2}{E_2} \quad (2)$$

where E_1 , E_2 represent Young's modulus of the roller and the raceway, respectively, MPa; ν_1 , ν_2 , the Poisson ratio of the roller and groove material; δ , deformation of a single roller; Q_n , force acting on a single roller, N; l_e , length of roller, mm; η , parameter that depends on E and ν .

This research adopted the linear rolling guide produced by the company of THK. Parameters of the guide rail are shown in Table 1.

Table 1. Parameters of linear rolling guide [17].

Parameters	Value
Young's modulus E_1, E_2 [GPa]	206
Poisson ratio ν_1, ν_2	0.3
Length of roller l_e [mm]	8
The diameter of the roller d [mm]	4
The number of single row roller Z	21

Substituting the parameters into (1), the relationship between the deformation δ of the roller and the load Q_n was obtained. The stiffness curve shown in Fig.3. is plotted. The roller contact stiffness $K=2.77 \times 10^5$ N/mm was obtained by

the linear fitting method. On the other hand, K is also the stiffness of the spring element in the finite element model.

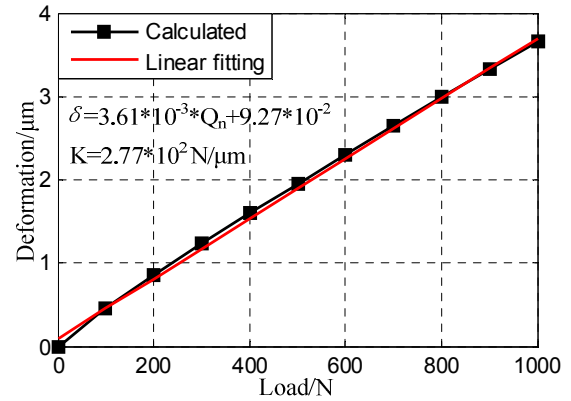


Fig.3. The stiffness curve of roller.

B. Finite element model of guide rail and slide block

A contact element was used to model the contact phenomena and the elasticity of a single roller. With regard to the physical modeling, each roller was equivalent to a spring element, which connects the slider with the guide rail in the finite element model. The idea of modeling is shown in Fig.4.

The roller contact stiffness calculated by (1) and (2) was assigned to the spring element. When Q_n was lower than zero, the gap occurred between the roller and raceway. Therefore, the elastic of spring element was zero in the finite element model. When Q_n was greater than zero, the deformation occurred between the roller and raceway. The elastic of spring element was K ($K=2.77 \times 10^5$ N/mm) in the finite element model. The reference length of the spring was equal to the diameter of the roller. Generally, the diameter of the roller should be slightly larger than the normal spacing, so that the roller and the raceway surface will produce interference fit.

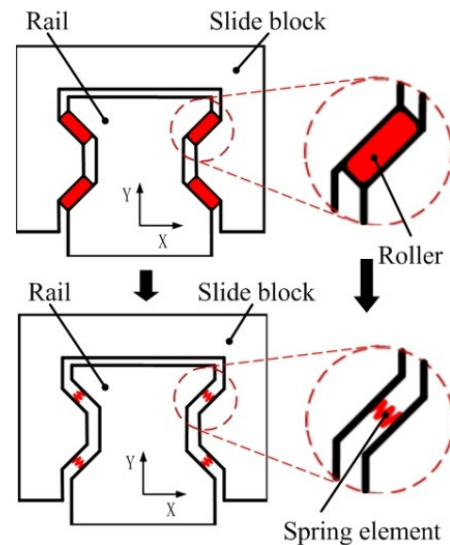


Fig.4. The roller was replaced by the spring element.

Necessary geometric dimensions and preload for the slider were taken from the product list [17]. Preload was $0.08C$; C is the dynamic capacity and equals to 22.8 kN. Dividing the preload by the number of rollers, the load subjected to each roller could be obtained. Based on the characteristics described by (1), the deformation δ of each roller was $2\ \mu\text{m}$. It is possible to increase the spring element reference length by $2\ \mu\text{m}$ to simulate the preload.

As shown in Fig.5., the coupling constraints were established between the end points of the spring element and the contact areas of the raceway. The coupling nodes shared the load. The Young's modulus of guide rail and slider block were 206 GPa, the Poisson ratio was 0.3. The guide rail and slider block were meshed with hexahedron, and obtained a total of 120 122 elements and 133 738 nodes.

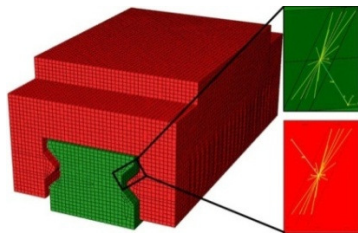


Fig.5. Finite element model of guide rail and slide block.

In the finite element model, the base of the guide rail was fixed. A load of 0 to 30 kN was applied to the upper surface and the side surface of the slide block, respectively. In order to avoid the stress concentration, the concentrated force was transformed into the pressure distributed on the surface. The displacements of slider in vertical and horizontal direction were extracted, so the stiffness curves of slider were obtained.

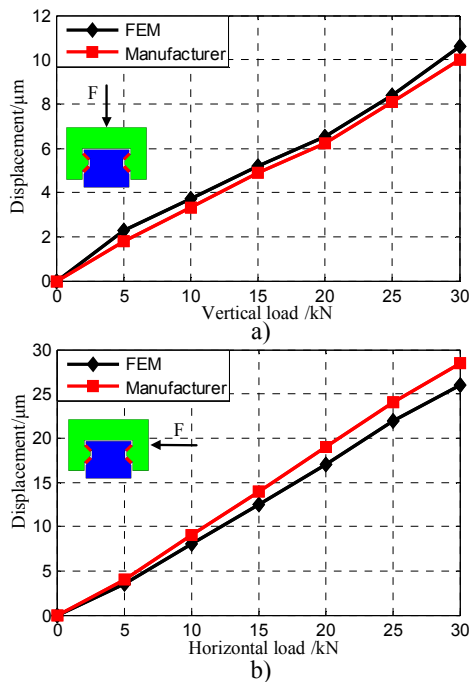


Fig.6. Comparison of slider stiffness curves.

As shown in Fig.6., the stiffness curves obtained from finite element analysis and provided by the guide rail manufacturers were compared [17]. It could be seen from the figure that the two curves basically coincided. The difference was in the range of 4.8 %~10.2 %. Therefore, it could be considered that the achieved qualitative and quantitative conformity were high. The correctness of the finite element model of guide rails was proved.

C. Integrated finite element model

The integrated finite element model consists of guide rails, slide blocks, and test plate. A fixed constraint was applied to the base of the rail. The material of the test plate was gray cast iron with Young's modulus of 157 GPa, Poisson ratio of 0.27 and density of 7800 Kg/m³. The tetrahedral element was used for meshing. The finite element model of test plate consisted of 3 765 elements and 7 265 nodes.

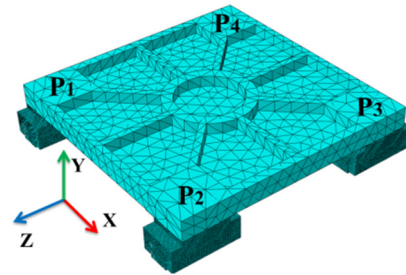


Fig.7. Integrated finite element model.

The bottom surface of the test plate and the upper surface of the slide block were tied together. Because the mesh size of the test plate was larger than slide blocks, the former was taken as a master surface and the latter was taken as a slave surface. The integrated finite element model is established in Fig.7., where P₁, P₂, P₃, P₄ are the serial numbers of the sliders. In the finite element analysis, the boundary condition of the guide rails was changed to make the slide blocks move in the X and Y directions so as to analyze the influence of geometric errors on the stress state of the test plate.

Due to the defects in the casting process, the material distribution was uneven. In the modeling process, the tiny characteristics of the test plate were neglected, which led to the deviation between the finite element model and the actual model. By comparing the measured strain and the strain obtained from the finite element analysis, Young's modulus and density of the test plate were modified repeatedly in the finite element model. Finally, Young's modulus and density were determined to be 126 GPa and 7450 Kg/m³.

4. SELECTION OF THE KEY MEASUREMENT POINTS ON TEST PLATE

The stress state of the test plate is related to the relative displacements of slide blocks. The relative displacements of slide blocks equal to the variation of the guide rail geometric errors. As shown in Fig.8., the slide blocks move along the Z axis, with the fourth slide block as the benchmark.

Consequently, we can obtain the displacements $\Delta x_1, \Delta y_1, \Delta x_2, \Delta y_2, \Delta x_3, \Delta y_3$ of the P_1, P_2, P_3 slide blocks relative to the benchmark. Based on the finite element model, the stress state of the test plate was analyzed when the relative displacements of the slide blocks were changed.

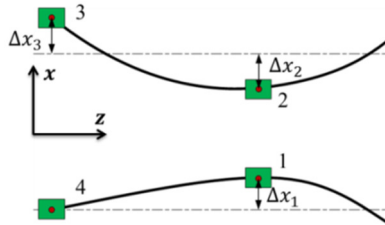


Fig.8. Relative displacements between slide blocks.

A. The key measurement points

With the change of the geometric errors, the relative position of slide blocks in the direction of X and Y will be changed, which leads to the deformation and the stress on the test plate [18]-[19]. But the stress was not evenly distributed. It was impossible to paste the strain gages at each location during the actual measurement process. Therefore, it was necessary to select some key measurement points. The stress at the points can adequately represent the stress state of the test plate and reflect the relative displacements of slide blocks.

The stress nephograms in Fig.9.a) and Fig.9.b) were obtained by changing the boundary conditions of the rails in the finite element model, making $\Delta y_2=5 \mu\text{m}$, and the rest remained unchanged. Let $\Delta x_2=5 \mu\text{m}$ and $\Delta y_2=-5 \mu\text{m}$ to obtain the stress nephogram in Fig.9.c) and Fig.9.d).

Considering the stress state of the test plate, the positions where the stress changes more significantly were selected as the key measurement points as shown in Fig.10. The stress σ_x in the X direction was measured at positions 2, 4, 6, 8, 10, 12, 14, 16. Among them, 4, 8, 12 and 16 were located on the bottom of the test plate. The stress σ_z in the Z direction was measured at positions 1, 5, 9, 13. And the stress σ_{xz} along the direction of the 45° ribs was measured at positions 3, 7, 11 and 15.

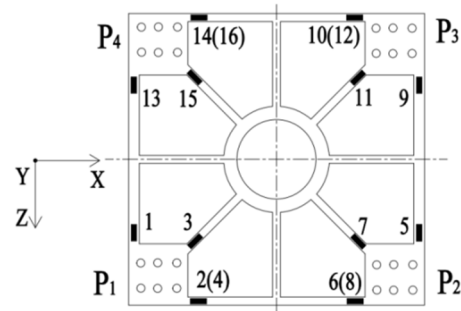


Fig.10. The key measurement points.

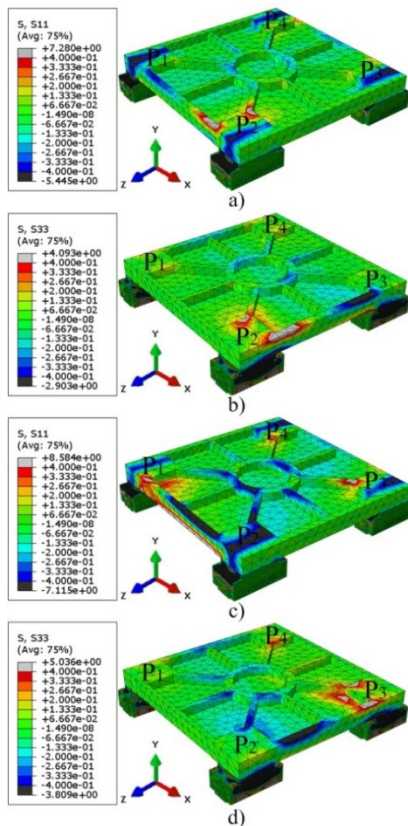


Fig.9. The stress nephogram of the test plate when the boundary conditions of the guide rails were changed. a) and c): the stress along the X direction, b) and d): the stress along the Z direction.

B. Resolution of measurement system

The measurement system consists of resistance strain gages, strain tester and static signal acquisition system. It was used to measure the strain at each key measurement point. From the knowledge of mechanics of materials, the relationship between stress σ and strain ϵ was:

$$\sigma = E \epsilon \quad (3)$$

where E presents Young's modulus of the test plate. Thus, the stress values at key measurement points can be obtained by (3).

Based on the integrated finite element model, a vertical downward displacement was applied to the guide rail at the position P_2 of the test plate. The displacement increases monotonically in the range of 1~10 μm , and the other positions of the guide rails did not impose displacement. The strain curves which were obtained by finite element analysis are plotted in Fig.11.

The results of finite element analysis show that only at points 2, 4, 5, 6, 7, 8 and 9 there is obvious strain. In other words, the strains at the other points were very small. As the test plate only has a bending strain, there is no tensile strain. The absolute value of the strain at points 4, 8 was equal to points 2, 6. Thus, it is not shown in Fig.11.

It can be seen from Fig.11. that 1 $\mu\epsilon$ was generated at the part of key measurement points on the test plate when the relative displacements of slide block were increased by 2 μm . The resolution of the resistance strain gage used in the measurement system was 1 $\mu\epsilon$, while the strain tester had a resolution of 0.1 $\mu\epsilon$. In other words, the resolution of the

measurement system was 2 μm . If a Wheatstone bridge or a higher resolution strain gage were used, the measurement system could identify a smaller relative displacement of slide blocks.

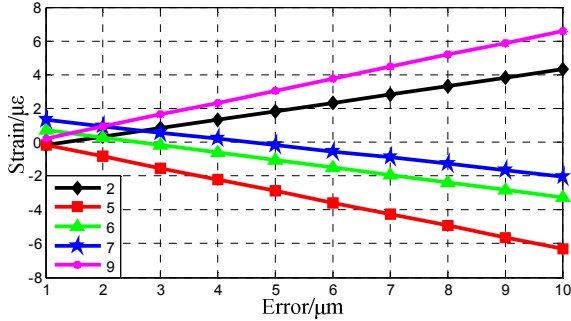


Fig. 11. The change of strain curves.

5. BP NEURAL NETWORK

Nowadays, the neural network has become a more effective learning technique in pattern recognition areas. The neural network has a strong ability to learn and self-organize information. It only needs a few specific requirements and prior assumptions for modeling. These advantages have attracted much interest in the research of the machine error identification [20]-[21].

The stress state of the test plate is affected by the relative position of the four sliders. But it is difficult to calculate the stress of each point on the test plate by the relevant shell theory. Furthermore, there is a dynamic joint between the guide rail and the slider, and a static joint between the slider and the test plate too. Thus, it is difficult to establish the mathematical model between the stress and the geometric errors accurately. In this case, BP neural network is chosen to establish the mapping relationship between the stress and the guide rail geometric errors.

A. BP neural network

BP neural network does not need to know the structure and parameters of the object. Through the training of a number of learning samples, the mapping relationship between the input and output can be established. Fig.12. represents the structure of the neural network model including input layer, output layer and hidden layer.

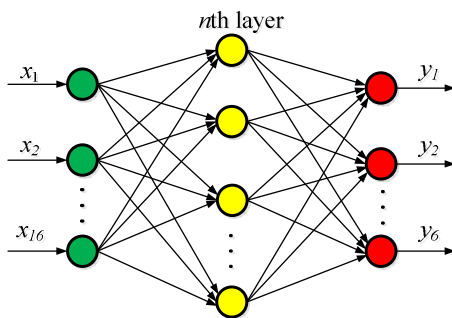


Fig. 12. Structure of BP neural network.

Suppose there are m nodes in the input layer, l nodes in the output layer, and p nodes in the n th hidden layer. Taking the j th neuron of the n th layer as an example, the neuron has many inputs x_j^{n-1} which come from the neurons in the $(n-1)$ th layer, but only a single output x_j^n that carries its signal to the neurons in the $(n+1)$ th layer [22]. An adjustable weight, w_{ij}^n , represents the connecting strength between the i th neuron of the $(n-1)$ th layer and the j th neuron of the n th layer. The output of the neural network is denoted as y_k ($k=1, 2, \dots, l$).

The hyperbolic tangent was selected as the transfer function of the neuron:

$$f(x) = \tanh(x) = \frac{1 - \exp(x)}{1 + \exp(x)} \quad (4)$$

Mathematically, the sum of the j th neuron net_j^n in the n th layer can be expressed as:

$$net_j^n = \sum_i w_{ij}^n x_i^{n-1} - \theta_j^n \quad (5)$$

where θ_j^n was an internal threshold of the j th neuron. The output value x_j^n can be calculated as:

$$x_j^n = f(net_j^n) = \frac{1 - \exp(-net_j^n)}{1 + \exp(-net_j^n)} \quad (6)$$

From (4), (5) and (6), we can calculate the internal threshold θ_j and the adjustable weight w_{ij} of the neurons based on the input x_i . The training process is finished if the total error between the calculated output y_k and the desired output y_p is less than the given error value. Otherwise, θ_j and w_{ij} were adjusted according to the error back propagation algorithm.

The stress value $S_i(\sigma_1, \sigma_2, \dots, \sigma_{16})$ of the key measurement points in the finite element model was taken as the input and the slide block relative displacements $\Delta_i(\Delta x_1, \Delta y_1, \Delta x_2, \Delta y_2, \Delta x_3, \Delta y_3)$ were taken as the output. The BP neural network model was established using MATLAB as shown in Fig.12. The number of input and output nodes was 16 and 6, respectively. The number of hidden layers and nodes in each hidden layer were generally determined by a lot of experiments. After repeated experiments, the hidden layer was determined to be 2 layers and the number of nodes in the hidden layer was 12 and 8, respectively.

B. Training of BP neural network

Before the training of the BP neural network, we must first collect learning samples. The orthogonal test has the characteristics of neat comparability and equilibrium dispersion [23]. It can obtain more comprehensive samples as few as possible. Eight values of the displacement $\Delta x_1, \Delta y_1, \Delta x_2, \Delta y_2, \Delta x_3$ and Δy_3 were taken with respect to the reference sliders in the respective feasible domains. The orthogonal table $L_{64}(8^9)$ was selected and there were 64 groups of learning samples. The learning samples were

obtained from the finite element model and the randomly selected 15 groups as the test samples. In order to accelerate the convergence of BP neural network, the learning samples should be normalized before training.

The maximum number of learning was 50,000, the learning rate was 0.01 and the permissible error was 10^{-6} . After the training of BP neural network, the test samples were used to test it. The results show that the difference is within 8 % as shown in Table 2. In this case, the mapping $f(\bullet)$ between S_i and Δ_i was established by $\Delta_i = f(S_i)$.

Table 2. Comparison of results.

	Output [μm]	Desired [μm]	Error [%]
Δx_1	5.3	5	6%
Δy_1	3.2	3	6.7%
Δx_2	-4.2	-4	5%
Δy_2	-5.4	-5	8%
Δx_3	8.5	8	6.3%
Δy_3	4.2	4	5%

The relative displacements of slide blocks $\Delta_i(\Delta x_1, \Delta y_1, \Delta x_2, \Delta y_2, \Delta x_3, \Delta y_3)$ can be obtained by inputting the stress values $S_i(\sigma_1, \sigma_2, \dots, \sigma_{16})$ into the trained BP neural network, and then getting a series of discrete points Δ_i . After the data processing, the geometric errors of two guide rails in the X and Y directions can be obtained.

6. EXPERIMENTAL VERIFICATION

The BP neural network demonstrates the mapping relationship between the stress values $S_i(\sigma_1, \sigma_2, \dots, \sigma_{16})$ and the relative displacements $\Delta_i(\Delta x_1, \Delta y_1, \Delta x_2, \Delta y_2, \Delta x_3, \Delta y_3)$ of slide blocks. The measured stress values at the key measurement points of the test plate are input into the trained BP neural network. And the relative displacements of slide blocks which were obtained from the BP neural network are compared with the measured geometric errors. Thus, the correctness of the integrated finite element model and the practicability of BP neural network were verified.

A. Geometric error measurement of guide rails

As shown in Fig.13.a), the straightness of the two guide rails in the X and Y directions was measured by the

photoelectric auto-collimator, respectively. The reflector was attached to the upper surface of the slide block. And the measuring light path between the reflector and the photoelectric auto-collimator was adjusted [24]. Move the slide block to the starting position and set the position as the reference point in the photoelectric auto-collimator. Move the slide block 100 mm at a time. The data was collected after the signal of the photoelectric auto-collimator stabilized. Thereby, we can obtain the straightness of each guide rail in the X and Y direction.

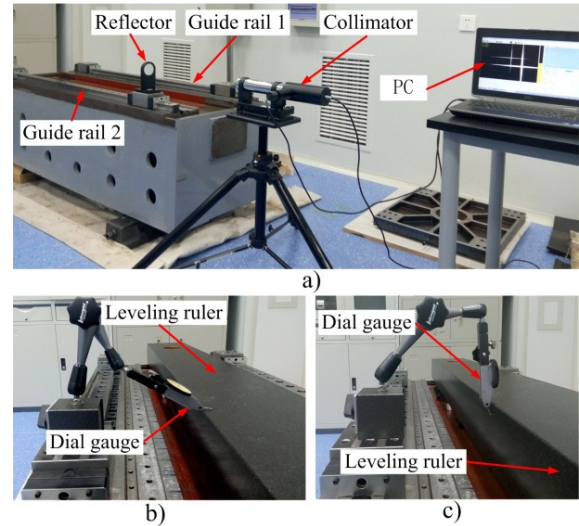


Fig.13. Guide rail geometric error measurement.

The high-precision leveling ruler and high-sensitivity dial gauge was used to measure the parallelism between the two guide rails. In Fig.13.b) and Fig.13.c), the leveling ruler was laid on the test bench and used as the measurement reference. The dial gauge was attached to the slide block, and the pointer was in contact with the top and side surface of the leveling ruler, respectively. Measurements were made from the starting position. The slide block was moved 100 mm at a time and then read the dial gauge. The above measurement procedure was repeated three times and the average value was taken. Taking the guide rail 1 as the benchmark, the geometric errors of the two guide rails in the X and Y direction can be obtained, as shown in Fig.14.

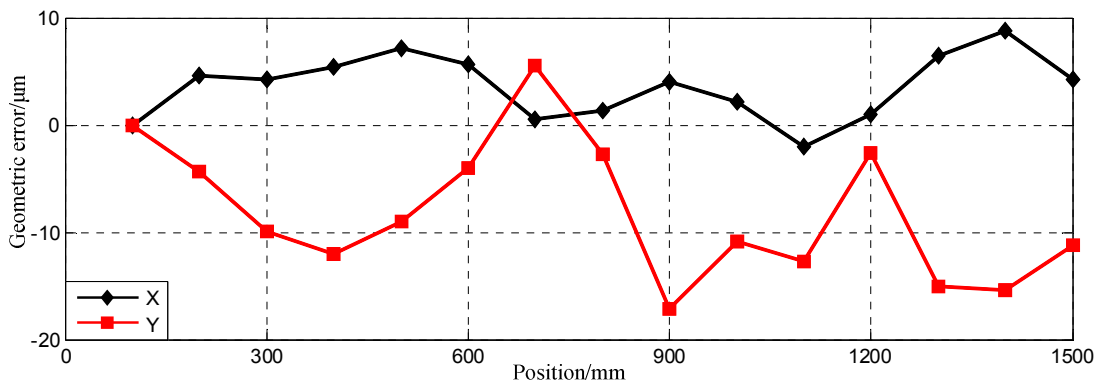


Fig.14. Geometric errors in the X and Y direction.

B. Stress measurement

The test plate was first bolted to the four slide blocks and a torque of 40 N•m was applied to the bolt with a torque wrench. Attach the strain gage to the surface of test plate and ensure that the orientation of the strain gage corresponds to the direction shown in Fig.10. Since the experiment was carried out in a constant temperature environment of 20 ± 0.5 °C, no temperature compensation was required [19].

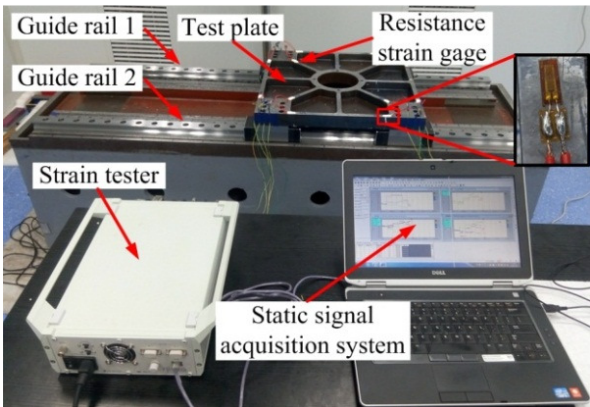


Fig.15. The stress measurement process.

The test plate was moved to the starting position. Then we balanced each channel and cleared the zero point. The test plate moved 100 mm every time. The data was collected after the signal was stable. By filtering out the interference

signals during the measurement process, the strain relative to the starting position of the test plate can be obtained throughout the trip. The measurement process was repeated three times in order to obtain the average value of strain. The strain value was converted into stress according to (3).

Then we changed the tightening torque of the bolts. A tightening torque of 60 N•m was applied to the bolts with a torque wrench and the above measurement process was repeated. Comparing the stress values under different bolt tightening torques, it was found that the tightening torque of the bolts has little effect on the measurement results. In other words, bolt tightening torque has little influence on the relative displacement between slide blocks.

C. Comparison of the results

The stress values collected by the measurement system were input into the trained BP neural network to obtain the relative displacement of slide blocks. Taking the guide rail 1 as the benchmark, the relative displacements were converted into the geometric errors of the two guide rails in the X and Y directions.

In the X direction, the maximum error between the output value of BP neural network and the measured value was 4.2 μm . The maximum error value in the Y direction was 5 μm . Comparing the error curves in Fig.16.a) and Fig.16.b), we learned that the established BP neural network was practical. And the mapping relationship between the stress of the test plate and the geometric error of guide rail can be established by BP neural network.

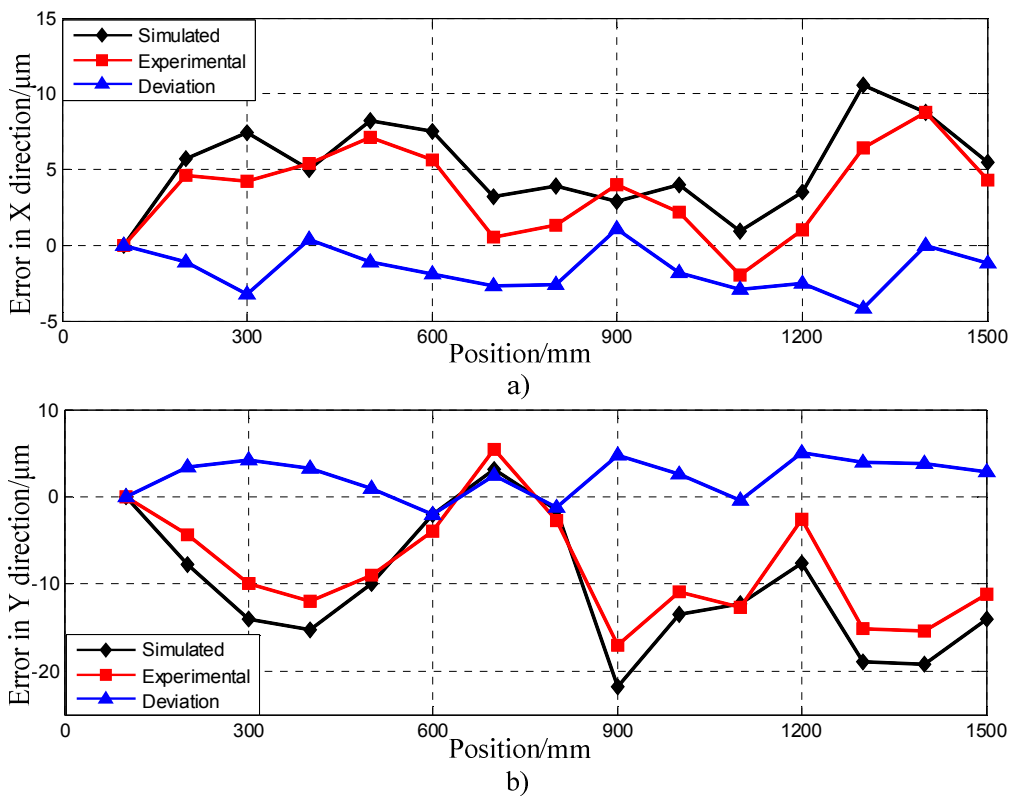


Fig.16. The output of the BP neural network and the measured geometric errors.

D. Geometric error adjustment

According to the results obtained from BP neural network, the geometric errors of the two guide rails in the X and Y directions were adjusted. The geometric errors in the X direction can be adjusted by adjusting the screw of the wedge plate or lapping the side mounting surface of the guide rail [6]. For the geometric errors in the Y direction, we generally use the scraping rail mounting surface to adjust the geometric errors.

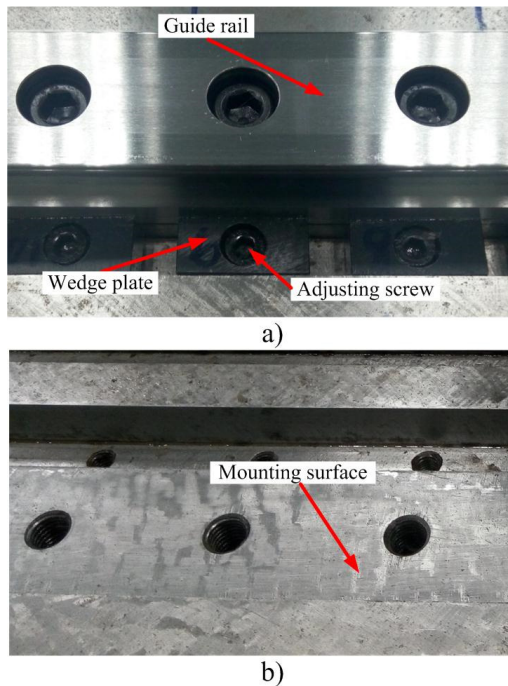


Fig.17. The adjustment of geometric errors.

When the geometric errors adjustment was completed, the stress at each key measuring point of the test plate was measured again. Then inputting the measured stress into the BP neural network, we can get the geometric errors in the X and Y direction again. According to the obtained error curves, the geometric errors of the guide rail were adjusted again until the stress did not exist at each key measurement point. At this time, the additional load of slide blocks during the movement was greatly reduced, which was helpful to improve the service life of the guide rail and the motion precision of the table.

7. CONCLUSION

A new method for guide rail geometric error identification and adjustment has been proposed. In finite element model, the sub-assemblies were discretized with solid elements and the roller was replaced by the spring element. Through the finite element analysis of the self-designed test plate, sixteen points on the surface of test plate were selected as the key measurement points, which the stress changed more significantly. The mapping relationship between the stress of the test plate and the geometric errors of the guide rail was established by using the BP neural network. The data

extracted from the finite element model was used as the learning samples to train the BP neural network. The test error was no more than 10 %, indicating that the BP neural network has good generalization ability. Compared to the geometric errors that we obtained from BP neural network and the measurement, the maximum difference was 4.2 μm and 5 μm in the X and Y direction, respectively. In conclusion, the proposed method can accurately identify the geometric errors of the guide rail and provide reference for geometric errors adjustment.

ACKNOWLEDGMENT

This research project is supported by the National Natural Science Foundation of China (No.51675378) and the National Science and Technology Major Project of China (No.2015ZX04005001).

REFERENCES

- [1] Okafor, A.C., Ertekin, Y.M. (2000). Derivation of machine tool error models and error compensation procedure for three axes vertical machining center using rigid body kinematics. *International Journal of Machine Tools & Manufacture*, 40 (8), 1199-1213.
- [2] Tian, W., Gao, W., Zhang, D., Huang, T. (2014). A general approach for error modeling of machine tools. *International Journal of Machine Tools & Manufacture*, 79 (4), 17-23.
- [3] Ohta, H., Tanaka, K. (2010). Vertical stiffnesses of preloaded linear guideway type ball bearings incorporating the flexibility of the carriage and rail. *Journal of Tribology*, 132 (1), 547-548.
- [4] Rahmani, M., Bleicher, F. (2016). Experimental and numerical studies of the influence of geometric deviations in the performance of machine tools linear guides. *Procedia CIRP*, 41, 818-823.
- [5] Shamoto, E., Park, C.H., Moriwaki, T. (2001). Analysis and improvement of motion accuracy of hydrostatic feed table. *CIRP Annals - Manufacturing Technology*, 50 (1), 285-290.
- [6] Khim, G., Park, C.H., Shamoto, E., Kim, S.W. (2011). Prediction and compensation of motion accuracy in a linear motion bearing table. *Precision Engineering*, 35 (3), 393-399.
- [7] Khim, G., Oh, J.S., Park, C.H. (2014). Analysis of 5-DOF motion errors influenced by the guide rails of an aerostatic linear motion stage. *International Journal of Precision Engineering and Manufacturing*, 15 (2), 283-290.
- [8] Kim, G.H., Han, J.A., Lee, S.K. (2014). Motion error estimation of slide table on the consideration of guide parallelism and pad deflection. *International Journal of Precision Engineering and Manufacturing*, 15 (9), 1935-1946.
- [9] Li, J., Mao, K., Chen, Q., Nie, Y. (2015). Experimental research of large components of machine tools assembly stress distribution under different assembly process. *Machine Tool & Hydraulics*, 43 (21), 118-122.

- [10] Bosetti, P., Bruschi, S. (2012). Enhancing positioning accuracy of CNC machine tools by means of direct measurement of deformation. *The International Journal of Advanced Manufacturing Technology*, 58 (5), 651-662.
- [11] Liu, Y., Liu, M., Yi, C., Chen, M. (2014). Measurement of the deformation field for machine tool based on optical fiber Bragg grating sensors. In *International Conference on Innovative Design and Manufacturing*, 13-15 August 2014. IEEE, Vol. 971-973, 222-226.
- [12] Chlebus, E., Dybala, B. (1999). Modelling and calculation of properties of sliding guideways. *International Journal of Machine Tools & Manufacture*, 39 (12), 1823-1839.
- [13] Majda, P. (2012). Relation between kinematic straightness errors and angular errors of machine tool. *Advances in Manufacturing Science & Technology*, 36, 47-53.
- [14] Majda, P. (2012). Modeling of geometric errors of linear guideway and their influence on joint kinematic error in machine tools. *Precision Engineering*, 36 (3), 369-378.
- [15] Shi, Y., Zhao, X., Zhang, H., Nie, Y., Zhang, D. (2016). A new top-down design method for the stiffness of precision machine tools. *The International Journal of Advanced Manufacturing Technology*, 83 (9), 1887-1904.
- [16] Zhupanska, O.I. (2011). Contact problem for elastic spheres: Applicability of the Hertz theory to non-small contact areas. *International Journal of Engineering Science*, 49 (7), 576-588.
- [17] THK Co., Ltd. (2008). *THK Linear Motion System Catalog*.
- [18] Kowalik, M., Rucki, M., Paszta, P., Gołębski, R. (2016). Plastic deformations of measured object surface in contact with undeformable surface of measuring tool. *Measurement Science Review*, 16 (5), 254-259.
- [19] Gawedzki, W., Tarnowski, J. (2015). Design and testing of the strain transducer for measuring deformations of pipelines operating in the mining-deformable ground environment. *Measurement Science Review*, 15 (5), 256-262.
- [20] Fuh, K.H., Wang, S.B. (1997). Force modeling and forecasting in creep feed grinding using improved BP neural network. *International Journal of Machine Tools & Manufacture*, 37 (8), 1167-1178.
- [21] Basheer, I.A., Hajmeer, M. (2000). Artificial neural networks: Fundamentals, computing, design, and application. *Journal of Microbiological Methods*, 43 (1), 3-31.
- [22] Rafiq, M.Y., Bugmann, G., Easterbrook, D.J. (2001). Neural network design for engineering applications. *Computers & Structures*, 79 (17), 1541-1552.
- [23] Tsui, K. (2007). Strategies for planning experiments using orthogonal arrays and confounding tables. *Quality & Reliability Engineering*, 4 (2), 113-122.
- [24] Ekinici, T.O., Mayer, J.R.R. (2007). Relationships between straightness and angular kinematic errors in machines. *International Journal of Machine Tools & Manufacture*, 47 (12-13), 1997-2004.

Received February 02, 2017.

Accepted May 18, 2017.